

ASSESSING THE STRUCTURAL BEHAVIOUR OF TIMBER-STEEL COMPOSITE BEAMS USING DISTRIBUTED FIBRE OPTIC SENSORS

Brendan P.H. Deeves¹, Joshua Woods²

ABSTRACT: This paper presents the results of an experimental program aimed at quantifying the structural behavior of CLT-steel composite beams for the application of timber-steel composite floor systems. In North America and globally, there has been a significant increase in the need for design and construction practices that maximize efficiency and minimize greenhouse gas emissions. This study investigates the use of cross-laminated timber (CLT) in place of conventional concrete in composite floor systems. The goals of this study were to investigate the performance of post-installed shear connections composed of self-tapping screws and to quantify the behaviour of CLT-steel composite beams using distributed sensing technology. To accomplish these objectives, direct shear tests were performed on self-tapping screw shear connections to quantify their load-slip response and failure modes. Full-scale composite beam specimens with self-tapping screw shear connections were then tested under monotonic loading to study their load-slip behaviour, stiffness, ultimate capacity, and governing failure modes. Composite beams were instrumented with distributed fibre optic strain sensors, which allowed for an in-depth analysis of the strain distribution throughout the composite section. Results of this study indicate that CLT-steel composite beams are an efficient and sustainable floor system with a ductile response, and that distributed fibre optic sensors offer unparalleled insight into the behaviour of CLT-steel composite beams.

KEYWORDS: Cross-laminated timber, shear connection, distributed fibre optic sensing, timber-steel composite

1 – INTRODUCTION

Composite floor systems composed of steel beams and a concrete slab have long been used in construction due to their ease of construction and high strength-to-weight ratio. Recently, the construction industry has been faced with significant challenges, as there is a growing pressure to increase the speed and efficiency of construction while reducing greenhouse gas (GHG) emissions. Thus, sustainable composite floor systems that can be installed efficiently without temporary shoring are required. A suitable remedy to these challenges is the use of timber-steel composite (TSC) beams, whereby composite sections are created from steel beams and cross-laminated timber (CLT) slabs in place of conventional concrete slabs. Timber-steel composite sections boast the ability to be installed without temporary shoring and offer significant reductions in GHG emissions compared to the use of concrete [1], which is one of the most prominent contributors to GHG emissions in the building sector [2]. Thus, CLT is a lightweight, sustainable, and more efficient solution for composite floor systems compared to the use of concrete.

2 – BACKGROUND

Early research into the behaviour and design of steel-concrete composite (SCC) beams by [3-5] resulted in the formation of the fundamental approaches to calculating the ultimate moment resistance of composite sections. In general, this work established that the ultimate moment resistance can be calculated using an internal couple of tensile and compressive forces computed using the limit state stresses of the materials. The calculation of the internal couple relies on the understanding of the distribution of stresses in the cross section, the degree of composite action, the location of the neutral axis, and the geometry of the composite beam. In addition to the geometry, the width of the floor slab that is effective in flexure must be known. Currently, knowledge gaps remain surrounding the distribution of stresses and strains in CLT slabs in flexure, and the influence of CLT in tension, something that is not a concern with SCC beams (because concrete in tension is ignored). The degree of composite action achieved in the section relies on the stiffness of the shear connection between the two layers - in SCC sections these are typically provided in the form of channels or studs welded to the top flange of the beam and cast integrally with the concrete slab. The

¹ Brendan P.H. Deeves, Department of Civil Engineering, Queen's University, Kingston, Canada, 19bphd@queensu.ca

² Joshua Woods, Department of Civil Engineering, Queen's University, Kingston, Canada, joshua.woods@queensu.ca

design and behaviour of these connections has been well studied [6-8], but they are not necessarily useful in the design of steel-timber composite beams. Due to the nature of CLT as a floor slab, shear connectors cannot be efficiently pre-installed, meaning that the shear connection between the steel beam and CLT slab must be completed in-situ after the placement of the slab.

The concept of using hybrid timber-steel composite floor systems is not novel, and several recent studies have focused on quantifying the performance of varying shear connection types and their influence on the behaviour of full-scale composite beams. Research into the performance of varying timber-steel shear connections composed of self-tapping screws [9], and coach screws [10] has been completed. A small number of large-scale experimental studies on the structural performance of timber-steel composite beams have also been reported in the literature. The structural performance of timber-steel composite beams was assessed by [11-13] considering varying shear connection type and timber slab type, including laminated veneer lumber (LVL), CLT, and glue-laminated (glulam) timber. The vibration and long term performance of CLT-steel composite beams has also been studied [14,15].

Although these studies have quantified the behaviour of TSC beams, significant knowledge gaps remain in the fundamental understanding needed to develop general design methods that can be used effectively by practicing engineers.

Considering challenges discussed, as well as the recent emergence of timber-steel composite beams, little guidance on timber-steel composite beams exists for Canadian designers. Additionally, CLT is not currently recognized as a composite design method in either the Canadian wood design standards (CSA 086) or Canadian steel design standards (CSA S16) [16,17]. To address these knowledge gaps, the aim of this research is to study the behaviour of post-installed shear connections composed of self-tapping screws (STS) and glue and their influence on the structural behaviour of TSC beams. Additionally, this study aims to study the distribution of strains along the length of the beam and throughout the depth of the section to gain a thorough understanding of the strain behaviour of TSC beams, and the influence of shear connection stiffness on capacity. The specific objectives of this study are to: (1) conduct direct shear tests to quantify the load-slip behaviour of partially threaded STS, (2) experimentally evaluate the performance of TSC beams constructed with STS shear

connections with and without glue, and (3) use distributed fibre optic sensors to evaluate the strain distributions within the composite beams.

3 – PROJECT DESCRIPTION

3.1 PUSHOUT TESTS

To quantify the load-slip behaviour of the STS, direct shear tests (referred to as pushout tests in this work) were completed. Pushout specimens are composed of two CLT slabs fastened to a steel W-section with eight STS as seen in Fig. 1(a). The CLT used in this study is 5-layer Spruce-pine-fir CLT with an E1 stress rating according to CSA O86 [16]. Each layer is 35 mm thick, producing an overall thickness of 175 mm. Longitudinal layers are machine stress rated with a bending strength of 13.4 MPa and transverse layers are visually graded stud grade No. 3 [16]. The pushout specimens tested in this phase of the research used Assy Kombi STS, which is a partially threaded STS with a hexagonal head that tapers into an unthreaded shank. The key dimensions of the STS are shown in Fig. 1(b). The steel section used to construct pushout specimens was a W310x39 (Canadian designation) of Grade ASTM A992 [18]. Fig. 1(c) shows the placement of the screw relative to the steel flange. STS were spaced at 150 mm and installed in 11.1 mm (7/16 in.) holes in the steel section. 6 mm holes were predrilled in the CLT to receive the screw, and they were torqued to 36 Nm using a torque wrench before testing as per manufacturer specifications [19].

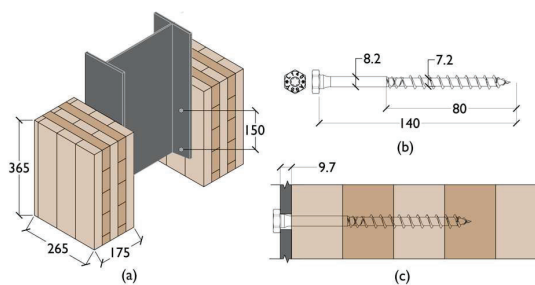


Figure 1. Pushout test specimen (a); 10×140 partially threaded STS (b); Position of screw relative to steel flange and CLT layers

3.2 COMPOSITE BEAM TESTS

Two composite beams were constructed and tested to failure in bending to assess the structural behaviour of TSC beams assembled with STS and a combination of glue and STS. A typical composite beam specimen is shown in Fig. 2, and the specimen details are summarized in Table 1. Both TSC beams are composed of a 5-layer

CLT panel oriented with its strong (major) axis parallel to the longitudinal axis of the steel beam. The grade and layup of the CLT panel is identical to that of the CLT used for the pushout specimens. The steel section used for TSC beam specimens was a W250×22 ($I_x = 28.9 \times 10^6 \text{ mm}^4$, $Z_x = 227 \times 10^3 \text{ mm}^3$) of grade ASTM A992 [18].

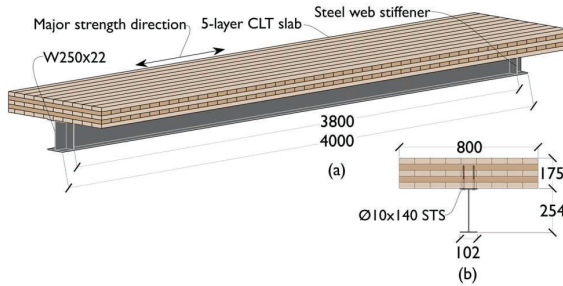


Figure 2. Composite beam specimen (a); Cross section (b)

Table 1: Composite beam specifications

Specimen	Span (mm)	STS (d×l)	STS Spacing (mm)	Glue-line thickness (mm)
Beam S	3800	10×140	100	-
Beam SG	3800	10×140	100	2.3

Material tests performed on coupons cut from the bottom flanges of the steel sections indicated that the average yield stress was 365 MPa (SD = 3.86 MPa) and the ultimate stress was 457 MPa (SD = 5.65 MPa). Both specimens were assembled with pairs of 10×140 mm partially threaded STS with a longitudinal spacing of 100 mm. STS were installed in 11.1 mm (7/16 in.) holes in the steel, 6 mm predrilled holes in the CLT, and tightened to 36 N-m using a torque wrench. The specimen constructed with STS and glue used PL Premium MAX adhesive, which is a commercially available bead extruded silane modified adhesive [20]. Three- 10 mm beads of adhesive were applied along the entire length of the CLT slab before placement of the steel beam and installation of STS. This adhesive was selected based on previous research on its use for composite beam shear connections conducted by [20].

Prior to the conduct of testing, composite beam specimens were instrumented with nylon coated distributed fibre optic sensors (FOS). Fig. 3 shows the FOS installed on the TSC beam and Fig. 4 shows the layout of the fibres. Fibres were bonded to both the longitudinal and transverse layers of the CLT, the bottom

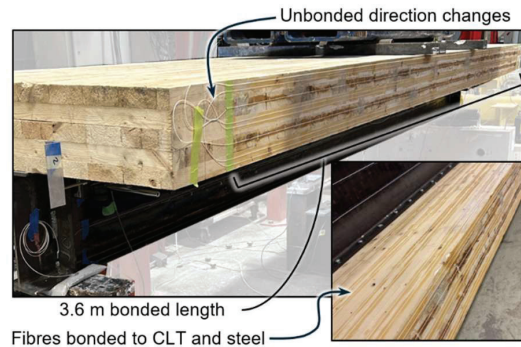


Figure 3. Fibre optic sensors installed on composite beams

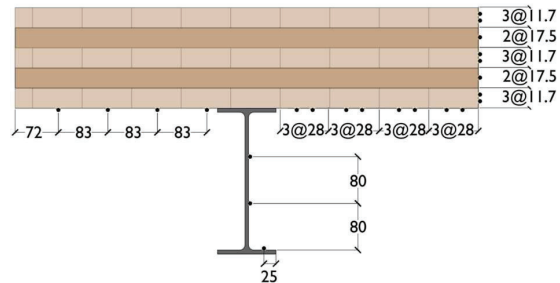


Figure 4. Fibre layout on composite beam cross section

of the CLT slab, and at three depths on the steel section – two on the web, and one on the inside of the bottom flange. FOS were bonded to the CLT using a two-component epoxy adhesive and bonded to the steel with a single-component cyanoacrylate adhesive. Fibres were installed over a length of 3.6 m, starting 0.1 m from each support. In total, approximately 80 m of fibre was installed on each specimen. With a gauge length of 2.6 mm, this represents over 30,000 discrete strain measurements, achieving a degree of fidelity that is not possible with the use of conventional discrete strain sensing technology.

4 – EXPERIMENTAL SETUP

4.1 PUSHOUT TESTS

Fig. 5 illustrates the test setup used for pushout specimens. Specimens were loaded in direct shear at a rate of 4 mm/min using a mechanical actuator with a capacity of 1200 kN. The load was applied through a 40 mm steel plate that was placed on top of the W-section, which ensured there was uniform load transfer. The load was measured using an internal load cell attached to the mechanical actuator and the relative slip between the steel and CLT was measured using four linear potentiometers (LP).

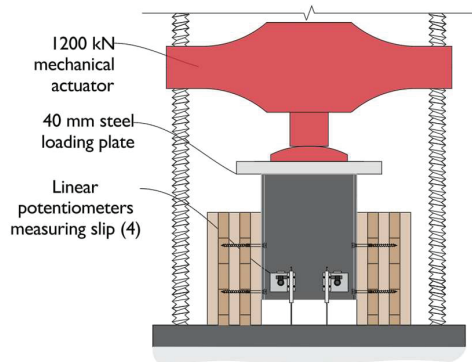


Figure 5. Pushout test setup

4.2 COMPOSITE BEAM TESTS

Fig. 6 shows the test setup used for composite beam tests. Specimens were loaded in four-point bending with simple support conditions over a span of 3.8 m, which was composed of two shear spans of 1.5 m and a constant moment region of 0.8 m. The load was applied with a 500 kN hydraulic actuator with a stroke of 150 mm. Two 100 mm wide steel bearing plates were installed at each support, and two 100 mm wide wood bearing plates were installed under each point load. The load was applied to the beam through two spreader beams, which were steel HSS 203×152×12.7 sections. Load measurements were recorded with a load cell. Midspan deflections were measured using four string potentiometers (SP). Two SPs were attached to the bottom flange of the steel section and two SPs were placed 150 mm from the outside edge of the CLT panel. This SP layout was selected to capture any rotation of the beam during testing. Four LPs were used to measure the relative slip between the steel and CLT at the ends of the beam. Strain readings were recorded using the Luna ODiSi 6400 fibre optic analyzer at a sampling rate of 1 Hz.

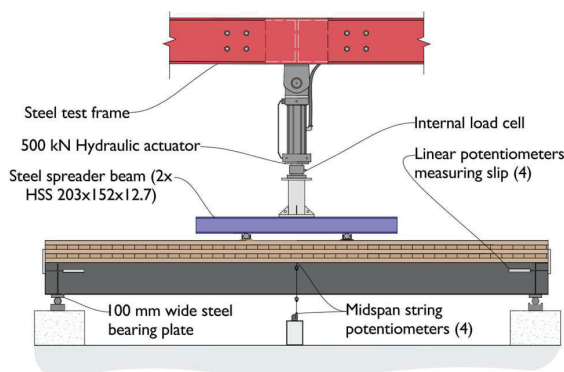


Figure 6. Composite beam test setup

5 – RESULTS

5.1 PUSHOUT TESTS

The load-slip results for the pushout specimens are summarized in Table 2 and shown in Fig. 7. The initial stiffness was calculated using the tangent stiffness of the load-slip response between 20 and 60 percent of peak load. These bounds were selected because the specimens were not preloaded before being tested to failure, meaning that the early load-slip response is distorted by the settlement of the CLT base, as well as stabilization of the screw within the predrilled holes in the steel.

Table 2: Summary of pushout test results

Specimen No.	Initial Stiffness (kN/mm)	Peak Load/STS (kN)	Slip at Peak Load (mm)
1	18.7	16.4	17.2
2	15.5	18.8	20.5

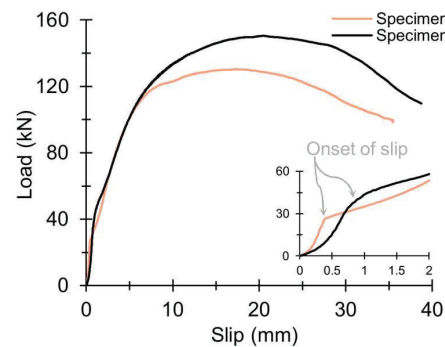


Figure 7. Load-slip response of 10×140 mm STS

The observed failure mechanisms of the shear connection are characterized by the crushing of wood parallel to the axis of loading, shown in Fig. 8(a), and plastic hinging of the STS, shown in Fig. 8(b). Note that the screw heads were cut off the STS shown in Fig. 8(a) to enable deconstruction of the specimens after testing and did not shear during testing. Plastic hinges formed at the shear interface between the CLT panel and the steel section and at the transition between the shank (unthreaded) and threaded portion of the STS. Thus, decreases in load carrying capacity were a result of a loss in stiffness in the connection without shearing the fastener. Significant ductility is observed in this shear connection, as a 20% drop in load is reached at approximately twice the displacement of the peak load.

Pushout tests for 10×140 mm STS indicate that the initial stiffness and peak load is variable, which is likely a result of local variations in wood density. The calculated stiffness of the shear connection for specimen 1 was 1.2

times that of specimen 2. Although this difference is significant, an investigation of the stiffness within the first 10 mm of slip (a reasonable interface slip at ultimate for a partially composite beam), shows only a 7% variation in secant stiffness. The peak load for both specimens is reached at an interface slip >15 mm, which indicates that the performance of this shear connection when implemented in a composite beam is likely controlled by its initial stiffness rather than the peak load carrying capacity.

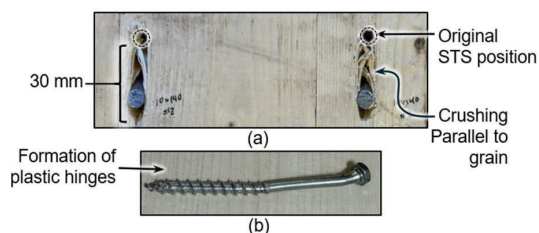


Figure 8. Crushing parallel to grain (a); Deformed STS (b)

5.2 COMPOSITE BEAM TESTS

Table 3 summarizes the parameters that characterize the structural response of the composite beams tested in this study. Fig. 9 and Fig. 10 show the load-deflection and load slip response of each specimen. The initial stiffness of the composite beams was calculated between 20 and 50 percent of the peak load. These bounds were selected to capture the elastic response of the composite beam between the initial slip of the shear connection and yielding of the steel section. The yield load was determined by defining a straight line between 40 and 90 percent of the peak load, and a new line that is tangent to the load-deflection curve and parallel to the tangent line between 40 and 90 percent of peak load. The yield load and deflection is taken by extending a line horizontally from the point of intersection of the initial stiffness with this new tangent to the load-deflection curve as described by [21].

The results shown in Fig. 9 indicate that both specimens exhibit an initial elastic pre-yield response. At a load of approximately 28 kN, the screwed connection begins to slip, which results in a slight decrease in stiffness relative to the elastic slope at loads below 28 kN. The results show that the initial stiffness of the composite beam can be greatly improved with the use of a combination of screws and glue, as the initial stiffness of Beam SG is 1.86 times that of Beam S. Both composite beams yield at a similar load, which was 173 kN for Beam S and 188 kN for Beam SG. The deflection at yield was 11 mm for Beam SG and 17 mm for Beam S. After yielding the steel,

the glue-line in Beam SG fractures. The onset of fracture occurred at a load of approximately 290 kN, and resulted in a 30 kN drop in load. The remainder of the glue-line fractured at a load of 321 kN, resulting in an approximate 31.5 kN decrease in load. Following the fracture of the glue-line, the interface slip measured for Beam SG was 4.15 mm at a load of 289 kN and the interface slip measured for Beam S was 4.1 mm at that same load. Thus, failure of the glue-line results in an instantaneous slip that is arrested by the STS and the resulting slip is identical to that of a shear connection with STS alone.

Table 3: Summary of composite beam test results

Specimen	Initial Stiffness (kN/mm)	Slip Load (kN)	Yield Load (kN)	Ultimate Load (kN)
Beam S	9.11	28	173	314
Beam SG	16.9	-*	188	321

*The screwed and glued connection did not slip before it fractured

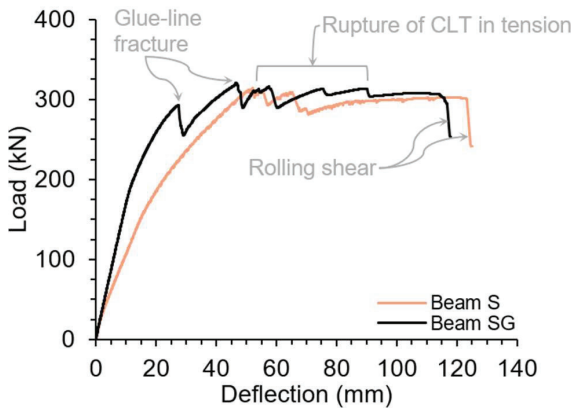


Figure 9. Load-deflection response of tested composite beams

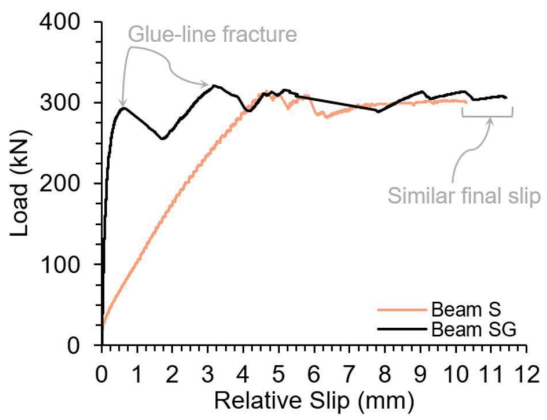


Figure 10. Load-slip response of tested composite beams

Beyond deflections of 50 mm, the CLT laminations on the underside of the slab began to rupture progressively

in tension (Fig. 11(a)), initiating at the extreme edge of the slab and propagating inward. The rupture of these layers did not result in a significant reduction in load carrying capacity, with the maximum reduction in load being approximately 10%. Relative slip between longitudinal layer of the CLT in contact with the steel and overlying layer of CLT was observed (Fig. 11(b)), which increased gradually throughout the test.

At deflections beyond 110 mm and a load of approximately 300 kN, both specimens experienced rolling shear failure, shown in Fig. 11(c) and Fig.11(d), which resulted in an approximate 20% decrease in load carrying capacity, at which point the test was terminated.

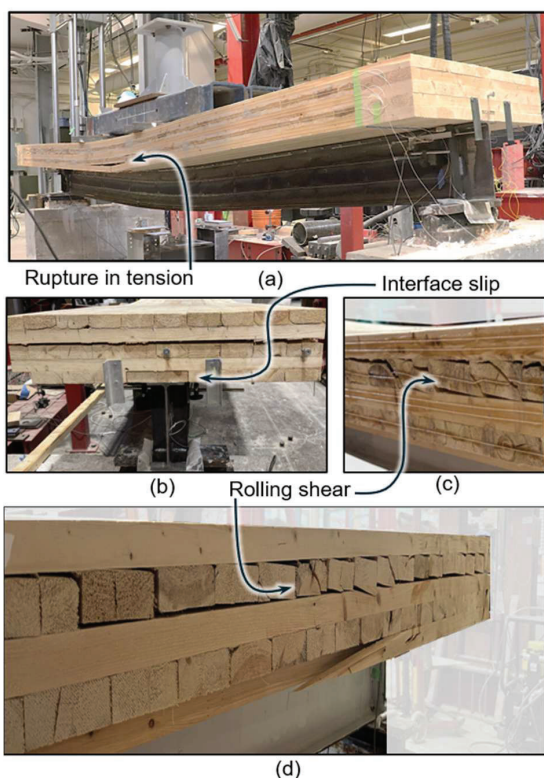


Figure 11. Rupture of CLT in tension (Beam S shown) (a); Interface slip (Beam S shown) (b); Rolling shear failure (Beam S shown) (c); Rolling shear failure (Beam SG shown) (d)

One of the primary objectives of this study was to gain a better understanding of the distributions of strains within TSC beams using distributed fibre optic sensors. Fig. 12 shows the distributed strain results at three load levels for each of the composite beams tested. The strain profiles shown along the length of the beam include the rows of fibre on the steel section and the longitudinal CLT layers.

The measured strain on the underside of the CLT panel and in the cross layers was omitted from these plots for clarity. The strain results along the length of the beams are summarized in three load levels (P): (1) $P = 20$ kN, which corresponds to a load that is smaller than the slip load of the STS shear connection, (2) $P = 150$ kN, which is at the onset of yielding of Beam S, and (3) $P = 220$ kN, which is a load stage where significant yielding of the steel sections has occurred.

In addition to the strain along the length of the beam, Fig. 12 shows the distribution of strain throughout the depth of the composite section. All strain profiles throughout the depth of the section were obtained by averaging the strain readings in the middle the constant moment region over a length of 200 mm. Thus, each strain profile through the depth of the section represents an average of 616 strain readings. The strain at the CLT-steel interface was determined by calculating the slope between the nearest two points in the CLT and steel and using linear extrapolation to the CLT-steel interface.

At a load of 20 kN the strain profiles for both composite beams, indicate that the neutral axis falls within the upper portion of the web of the steel section. Strain profiles in the steel are smooth and take a trapezoidal shape, which is expected based on the four-point bending conditions and the uniform material properties of the steel. Conversely, the strain profile for the CLT shows significant variations along the length of the beam. These inconsistencies are a result of local variations in the wood. Previous research conducted by [22] on strain distributions in glulam timber showed that the presence of knots, cracks, and finger joints can introduce significant variability in local strain distributions. At 20 kN (before the slip of the STS in Beam S) the strain profiles throughout the depth of the section are identical for both composite beams. Although the beams exhibit full composite action at this load level, a small discontinuity of approximately $40 \mu\epsilon$ is seen at the CLT-steel interface. This strain discontinuity is likely a result of the position of the fibres relative to the longitudinal axis, which will be discussed later in this paper.

At a load of 150 kN, the difference in performance between the STS shear connection and the STS and glue shear connection are more apparent. Beam S has reached the onset of yield, identified by the formation of local strain peaks in the constant moment region of the strain distribution. At this load, the tensile strains in the bottom flange of Beam S are 25% greater than that of Beam SG

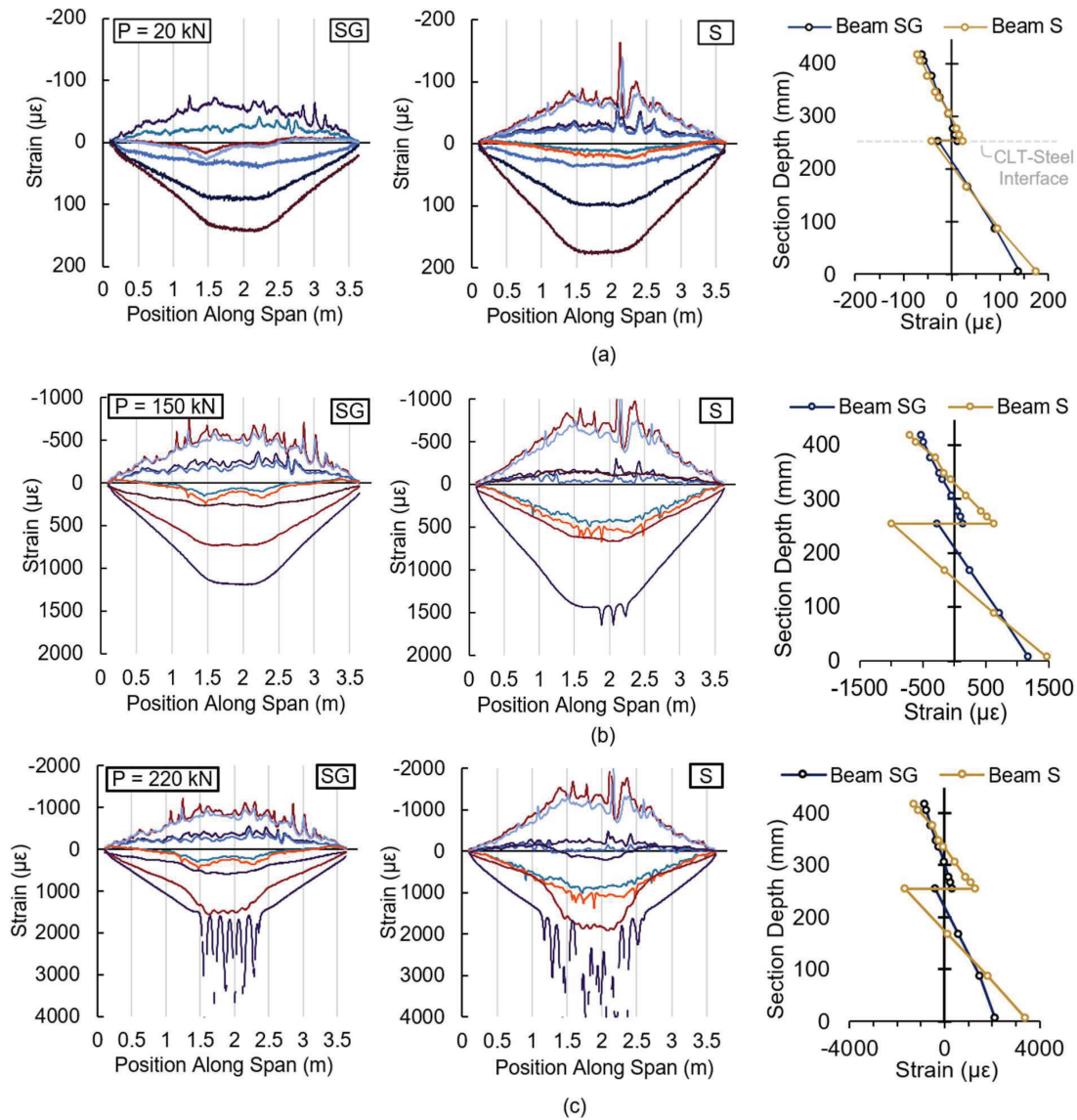


Figure 12. Strain along the length and through the depth of the composite beams at 20 kN(a); 150 kN (b); 220 kN (c)

and the neutral axis has shifted down in the steel section. Additionally, the STS shear connection in Beam S has slipped, and a significant loss in composite action is observed. Conversely, Beam SG is still exhibiting full composite action.

At the third load stage, 220 kN, both beams exhibit significant yielding in the steel section, but the glue-line in Beam SG has yet to fracture. Thus, the discontinuity in strain between the CLT and steel remains small and the CLT slab is predominantly in compression. For Beam S, the shear connection has continued to slip, and the underside of the CLT panel is subjected to significant tensile strains.

Fig. 13 shows the distribution of strain throughout the depth of the section at a load 300 kN, which is after the complete fracture of the glue-line in Beam SG. At this load, strains are well beyond yield in the steel section as the strains reach as high as 0.0025 at mid depth of the web. This strain behaviour agrees with previous observations, that, after the fracture of the glue-line, there is an instantaneous slip that is arrested by the STS. Upon loading, Beam SG then behaves in a manner that is nearly identical to that of Beam S, with the only difference being a slightly smaller strain discontinuity, which is attributed to increased interface friction due to the presence of glue.

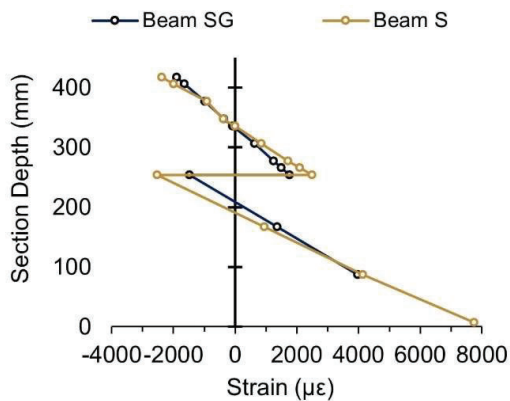


Figure 13. Strain profiles after glue-line fracture of Beam SG

At small loads, the load-slip response of the composite beams indicates that the sections are exhibiting full composite action. However, the strain profiles at these loads indicate that the section is not exhibiting full composite action. This contradiction is evident in the strain profiles previously shown at $P = 20$ kN. This load is before the slip of the STS shear connection in Beam S and before the fracture of the glue-line in Beam SG. At this load, the sections exhibit full composite action with ~ 0 interface slip. However, a noticeable discontinuity in strain is observed at the CLT-steel interface.

The interface strain discontinuities recognized in the analysis of strain profiles through the depth of the section can be investigated in more detail by the analysis of the distribution of strains across the width of the CLT slab. Fig. 14 shows the average strain on the bottom of the CLT slab in the middle 200 mm of the constant moment region for Beam S. Fig. 14 also shows the interface strain value extrapolated from fibres measuring the strain at the outside edge of the CLT slab.

In general, these results suggest that tensile strains are increasing as the distance from the longitudinal axis of the beam increases. This finding explains the reason for the appearance of a strain discontinuity at loads where the section is exhibiting full composite action. Since the fibres used to plot this profile were on the outside edge of the CLT slab, the plotted tensile strains are an overestimate of the actual behaviour of the CLT in the regions closest to the top flange of the steel section. This finding implies that the location in which strains are measured relative to the longitudinal axis of the beam can have a significant impact on the recorded strain data.

The strain distribution across the width of the CLT slab also explains the progressive rupture of the longitudinal

layers on the underside of the CLT slab. It was observed that the tension-side rupture of the CLT initiated at the outside edge of the slab and propagated inward. Based on these results, this behaviour was a result of the longitudinal layers towards the outside edge of the CLT slab reaching the rupture strain before the layers closer to the longitudinal axis of the beam.

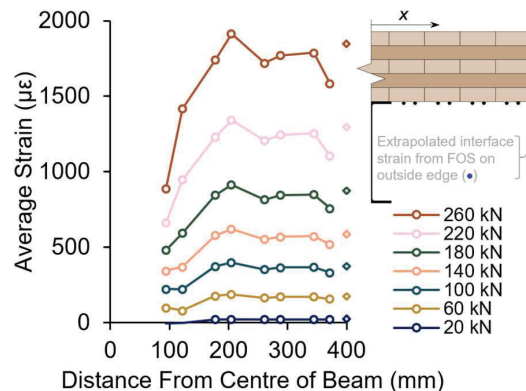


Figure 14. Average strain across the underside of the CLT slab in the middle 200 mm of the constant moment region (Beam S shown)

These findings highlight a fundamental challenge in strain measurement across all sensing technologies—the need for strategic fibre placement to accurately capture strain behaviour and to avoid misinterpretation of structural responses. This finding was only possible with the use of FOS, as they provide significantly higher resolution and continuous strain profiling compared to conventional methods.

6 – CONCLUSIONS

This paper presented an experimental campaign aimed at investigating the performance of post-installed shear connections for CLT-composite beams using self-tapping screws. Pushout tests were conducted to study the load-slip behaviour and failure mechanisms of STS shear connections. Two full-scale composite beams instrumented with distributed fibre optic sensors were tested in bending to study the influence of STS shear connections with and without glue and to quantify the structural behaviour of CLT-steel composite beams. The specific conclusions of this work are:

1. CLT-steel shear connections composed of partially threaded self-tapping screws form a relatively stiff and ductile connection.
2. The use of glue and screws in shear connections for CLT-steel composite beams

offers significant improvements to the initial stiffness of the composite beam and maintains composite action well beyond the yield load, but has little influence on ultimate capacity.

3. A shear connection composed of only self-tapping screws is effective at transferring the interface shear with moderate slip in the elastic region.
4. Distributed fibre optic sensors offer unparalleled insight into the distribution of strains along the length and throughout the depth of CLT-composite beams.

7 – ACKNOWLEDGEMENTS

The Authors would like to gratefully acknowledge funding provided by the Canadian Institute of Steel Construction (CISC) and the Natural Sciences and Engineering Research Council of Canada (NSERC). Technical assistance provided by Logan Callele is greatly appreciated. Technical support from Justin Bennett and Hal Stephens in the Structural Engineering Laboratory at Queen’s University is also acknowledged.

8 – REFERENCES

- [1] A. Younis and A. Doodoo. “Cross-laminated timber for building construction: A life-cycle-assessment overview.” In: *Journal of Building Engineering* 52 (2022), p. 104482.
- [2] Supriya, R. Chaudhury, U. Sharma, P. C. Thapliyal, and L. P. Singh. “Low-CO2 emission strategies to achieve net zero target in cement sector.” In: *Journal of Cleaner Production* 417 (2023), p. 137466.
- [3] Robinson, H. H.. “Composite beam incorporating cellular steel decking.” In: *Journal of the Structural Division* 95 (1969), pp. 355-380.
- [4] G. S. Vincent, A. Iron, S. I. C. of S. P. Producers, A. Iron, and S. I. C. of S. S. Producers, “Tentative criteria for load factor design of steel highway bridges.” American Iron and Steel Institute, Committee of Structural Steel Producers [and the] Committee of Steel Plate Producers, New York, N.Y., 1969.
- [5] W. C. Hansell and I. M. Viest. “Load Factor Design for Steel Highway Bridges.” In: *Engineering Journal* 8.4 (1971), Art. no. 4.
- [6] J. G. Ollgaard, R. G. Slutter, and J. W. Fisher. “Shear Strength of Stud Connectors in Lightweight and

Normal-Weight Concrete.” In: *Engineering Journal* 8.2 (1971), Art. no. 2.

- [7] R. G. Slutter and G. C. Driscoll. “Flexural Strength of Steel-Concrete Composite Beams.” In: *Journal of Structural Division* 91.2 (1965), pp. 71–99.
- [8] R. P. Johnson and R. J. Buckby, *Composite Structures of Steel and Concrete: Beams, columns, frames, and applications in building*. Crosby Lockwood Staples, 1975.
- [9] H. C. Merryday, K. Sener, and D. Roueche. “Pushout Tests on Steel-Timber Connections Using Self-Tapping Screws.” In: *Journal of Structural Engineering* (2023), pp. 312–327.
- [10] D. V. Bompa, A. Chira, and D. Zwicky. “Constitutive modelling of deformation rate dependent response of steel timber shear connections.” In: *Journal of Building Engineering* (2024), p. 111159.
- [11] A. Hassanieh, H. R. Valipour, and M. A. Bradford. “Experimental and numerical study of steel-timber composite (STC) beams.” In: *Journal of Constructional Steel Research* 122 (2016), pp. 367–378.
- [12] A. Hassanieh, H. R. Valipour, and M. A. Bradford. “Experimental and numerical investigation of short-term behaviour of CLT-steel composite beams.” In: *Engineering Structures* 144 (2017), pp. 43–57.
- [13] Ruyuan Yang, Jia Wan, Xiaofeng Zhang, and Youfu Sun. “Modelling of Steel-Timber Composite Beams: Validation of Finite Element Model and Parametric Study.” In: *Wood Research* 66.5 (2021), pp. 806–820.
- [14] A. A. Chiniforush, H. R. Valipour, M. A. Bradford, and A. Akbar Nezhad. “Experimental and theoretical investigation of long-term performance of steel-timber composite beams.” In: *Engineering Structures* 249 (2021), p. 113314.
- [15] A. A. Chiniforush, M. Makki Alamdari, U. Dackermann, H. R. Valipour, and A. Akbarnezhad. “Vibration behaviour of steel-timber composite floors, part (1): Experimental & numerical investigation.” In: *Journal of Constructional Steel Research* 161 (2019), pp. 244–257.
- [16] Canadian Standards Association (CSA), CSA O86: *Engineering design in wood*, Toronto, ON, Canada., 2024.

[17] Canadian Standards Association (CSA), CSA S16: Design and construction of steel structures, Toronto, ON, Canada., 2024.

[18] ASTM International, *ASTM A992/A992M-01: Standard specification for steel for structural shapes for use in building framing*, West Conshohocken, PA, USA, 2001.

[19] MyTiCon Timber Connectors, “MTC Installation Guide,” Surrey, BC, V3R 0E2 (2017).

[20] T. Hull, P. Ackerman, and D. Lacroix. “Development of a glue bonded shear connections aimed for mass timber composites.” In: *International Wood Products Journal* 15.2–4 (2024).

[21] Munoz, W., Mohammad, M., Salenikovich, A., and Quenneville, P. *Determination of Yield Point and Ductility of Timber Assemblies: In Search for a Harmonised Approach*. Engineered Wood Products Association, 2008.

[22] J. Goodwin, J. E. Woods, and N. A. Hout. “Assessing the structural behaviour of glued-laminated timber beams using distributed strain sensing.” In: *Construction and Building Materials* 325 (2022), p. 126844.